New Journal of Physics
The open-access journal for physics

Energy localization in maximally entangled two- and three-qubit phase space

Oktay K Pashaev[1,3] **and Zeynep N Gurkan**[2]

[1] Department of Mathematics, Izmir Institute of Technology, Urla-Izmir 35430, Turkey

[2] Center for Quantum Technologies, National University of Singapore, 117542 Singapore, Singapore

E-mail: oktaypashaev@iyte.edu.tr

New Journal of Physics **14** (2012) 063007 (24pp)
Received 13 June 2011
Published 7 June 2012
Online at http://www.njp.org/
doi:10.1088/1367-2630/14/6/063007

Abstract. Motivated by the Möbius transformation for symmetric points under the generalized circle in the complex plane, the system of symmetric spin coherent states corresponding to antipodal qubit states is introduced. In terms of these states, we construct the maximally entangled complete set of two-qubit coherent states, which in the limiting cases reduces to the Bell basis. A specific property of our symmetric coherent states is that they never become unentangled for any value of ψ from the complex plane. Entanglement quantifications of our states are given by the reduced density matrix and the concurrence determinant, and it is shown that our basis is maximally entangled. Universal one- and two-qubit gates in these new coherent state basis are calculated. As an application, we find the Q symbol of the XYZ model Hamiltonian operator H as an average energy function in maximally entangled two- and three-qubit phase space. It shows regular finite-energy localized structure with specific local extremum points. The concurrence and fidelity of quantum evolution with dimerization of double periodic patterns are given.

[3] Author to whom any correspondence should be addressed.

Contents

1. Introduction

Coherent states were first introduced by E Schrödinger, in the form of wave packets for the quantum harmonic oscillator, moving along the classical trajectories [1]. Then R J Glauber constructed these coherent states by the Heisenberg–Weyl group [2], for a description of coherent laser beams in quantum optics. Generalized coherent states for an arbitrary Lie group were invented by A Perelomov and some particular realizations of these states have been discussed by many researchers [3]. An important class of coherent states for the SU(2) and SU(1,1) groups describes spin waves in the Heisenberg spin model of ferromagnetism [4, 5]. The SU(1,1) coherent states have also been applied to superfluidity theory for the description of the Bogoliubov condensate state [7], in terms of pseudospin [5, 6]. It is impossible to mention here the uncountable number of papers devoted to the subject. We just observe that the coherent states for noninteracting magnons in spin models take the form of the direct product of Glauber's coherent states, which is a complete quantum analogue of the classical spin wave. The complete quantum analogue of the classical domain wall as a quantum state in the form of the Gaussian superposition of heavy spin complexes, as was shown by Gochev [8] using Jacobi's triple product identity, can be represented as a direct product of Bloch's coherent states. This state is a minimum uncertainty packet and the correlation functions in this state factorize. Quantum states in both the systems, noninteracting magnons and the quantum domain wall, are separable states.

Recently, in quantum information and quantum computation theory entangled coherent states became an interesting tool to study entanglement in quantum systems [14]. In this study, in addition to the Glauber coherent state $|\alpha\rangle$, another mirror-reflected state $|-\alpha\rangle$ has been introduced to construct entangled states like $|\alpha\rangle|\alpha\rangle + |-\alpha\rangle|-\alpha\rangle$ [9, 13]. However, these states

are not orthogonal $\langle -\alpha|\alpha\rangle = \mathrm{e}^{-2|\alpha|^2}$, and this creates several complications of computational and interpretational character. One can construct the even and odd coherent states [16], $(|\alpha\rangle \pm |-\alpha\rangle)/\sqrt{2}$, which are orthonormal but of course not complete. Entanglement of these Gaussian continuous-variable states (states with the Wigner function in the Gaussian form) has been demonstrated in an experiment of continuous-variable teleportation [10] and the quantification of entanglement for these states was given in [11, 12]. In contrast to the teleportation of a discrete quantum system, like a spin-1/2 particle state, in continuum-variable teleportation (as position and momentum), the teleportation process acts on an infinite-dimensional Hilbert space instead of the two-dimensional (2D) Hilbert space for the discrete spin variables. It was shown that the Peres–Horodecki criterion is a necessary and sufficient separability condition for all bipartite Gaussian states.

In this paper, motivated by the Möbius transformation and its action on symmetric points of the generalized circle in the complex plane, we introduce the complete set of spin-1/2 coherent states that are orthogonal and maximally entangled. The paper is organized as follows. In section 2, we pedagogically introduce the relations between the Möbius transformation and the qubit. We have paid special attention to the so-called symmetric points in the unit circle, appearing in the method of images from hydrodynamics, and to the related symmetric qubit quantum states. In section 3, we construct an orthonormal basis from symmetric antipodal qubit states and some elementary gates as Möbius transformations. Section 4 is devoted to the symmetric two-qubit coherent states. In section 5, we show that the set of states introduced in the previous section is maximally entangled. We follow three different methods: first we use the reduced density matrix method and the determinant method. Then we show that averages of spin operators in our states vanish. This property also confirms that our states are maximally entangled, according to another, operational definition of entangled states as maximally non-classical states. At first glance, since our states are continuous-variable states, the quantification of entanglement for these non-Gaussian states needs to be clarified. This is due to the fact that only the Gaussian states have been completely characterized for the case of continuous-variables. However, our states are defined in a high-dimensional Hilbert space; they have small Schmidt rank, namely 2, which we show by computing the reduced density operator at Bob's site. Therefore these states can local-unitarily be mapped to a two-qubit Hilbert space and their entanglement properties are thus not different from those of the two-qubit case. This justifies our use of concurrence in section 5. As an application of our results, in section 6 we calculate the average energy in our coherent states (Q symbol of H) for the two- and three-qubit cases in the XYZ model. This energy surface shows a regular character with local extremum points in maximally entangled two-qubit space. The time evolution of concurrence and the fidelity of our coherent states are derived in section 7. In section 8 we present some problems for future studies.

2. Linear fractional transformations and symmetrical quantum states

2.1. Möbius transformation and qubits

There is a well-known relation between the group of linear fractional transformations, or the Möbius transformations,

$$w = S(\psi) = \frac{a\psi + b}{c\psi + d}, \tag{1}$$

$ad - bc \neq 0$ and the group of two-by-two complex matrices [15]. Any matrix from the group, acting on states as

$$\begin{pmatrix} w_1 \\ w_2 \end{pmatrix} = \begin{pmatrix} a & b \\ c & d \end{pmatrix} \begin{pmatrix} \psi_1 \\ \psi_2 \end{pmatrix}, \tag{2}$$

in terms of the homogeneous coordinates $\psi = \psi_1/\psi_2$, $w = w_1/w_2$, implies fractional transformation (1). If we consider two quantum states $|\psi\rangle = \begin{pmatrix} \psi_1 & \psi_2 \end{pmatrix}^{\mathrm{T}}$ and $|w\rangle = \begin{pmatrix} w_1 & w_2 \end{pmatrix}^{\mathrm{T}}$ from 2D Hilbert space, related by a linear transformation $|w\rangle = U|\psi\rangle$, then it gives the fractional transformation (1) in the extended complex plane C.

In quantum computations, we have a qubit as a unit of information

$$|\psi\rangle = \begin{pmatrix} \psi_1 \\ \psi_2 \end{pmatrix}, \quad |\psi_1|^2 + |\psi_2|^2 = 1, \tag{3}$$

for which, in terms of the homogeneous coordinate $\psi = \psi_2/\psi_1$, we have

$$|\psi\rangle = \begin{pmatrix} \psi_1 \\ \psi_2 \end{pmatrix} = \psi_1 \begin{pmatrix} 1 \\ \psi \end{pmatrix}. \tag{4}$$

We fix ψ_1 by the normalization condition $\langle\psi|\psi\rangle = 1$, so that up to the global phase we have the qubit state as

$$|\psi\rangle = \frac{1}{\sqrt{1+|\psi|^2}} \begin{pmatrix} 1 \\ \psi \end{pmatrix}. \tag{5}$$

This state coincides with the spin-1/2 generalized coherent state [17]. From another side, for the qubit state

$$|\theta, \varphi\rangle = \cos\frac{\theta}{2}|0\rangle + \sin\frac{\theta}{2}\mathrm{e}^{\mathrm{i}\varphi}|1\rangle = \begin{pmatrix} \cos\frac{\theta}{2} \\ \sin\frac{\theta}{2}\,\mathrm{e}^{\mathrm{i}\varphi} \end{pmatrix} \tag{6}$$

determined by the point (θ, φ) on the Bloch sphere, parameterization by the homogeneous variable

$$\psi = \frac{\psi_2}{\psi_1} = \tan\frac{\theta}{2}\mathrm{e}^{\mathrm{i}\varphi} \tag{7}$$

gives stereographic projection of the point $(\sin\theta\cos\varphi, \sin\theta\sin\varphi, \cos\theta)$ on the unit sphere to the complex plane ψ [22]. Therefore the Bloch sphere can be considered as a Riemann sphere for the extended complex plane ψ and we have the $SU(2)$ or the spin-coherent state as

$$|\psi\rangle = \frac{|0\rangle + \psi|1\rangle}{\sqrt{1+|\psi|^2}}. \tag{8}$$

The computational basis states $|0\rangle = |\uparrow\rangle = (1 \quad 0)^{\mathrm{T}}$ and $|1\rangle = |\downarrow\rangle = (0 \quad 1)^{\mathrm{T}}$ in this coherent state representation are given just by particular points in the extended complex plane $(\Re\psi, \Im\psi) \cup \{\infty\}$, as $\psi = 0$ and $\psi = \infty$, respectively. One notes that these points are symmetric points with respect to the unit circle $\bar{\psi}\psi = 1$ at the origin.

2.2. Symmetric points

In complex analysis, two points ψ and ψ^* are called symmetric with respect to the circle C through ψ_1, ψ_2, ψ_3 if and only if $(\psi^*, \psi_1, \psi_2, \psi_3) = \overline{(\psi, \psi_1, \psi_2, \psi_3)}$, where the cross ratio of four points is

$$(\psi, \psi_1, \psi_2, \psi_3) = \frac{(\psi - \psi_2)\,(\psi_1 - \psi_3)}{(\psi - \psi_3)\,(\psi_1 - \psi_2)}. \tag{9}$$

The circle here is considered in the generalized form, that includes also a line, regarded as a circle with an infinite radius. On the Riemann sphere all generalized circles are coming from the intersection of the sphere with a plane, so that if the plane passes through the north pole, the corresponding projection would be a line. For the unit circle at the origin, we can choose $\psi_1 = -1$, $\psi_2 = \mathrm{i}$, $\psi_3 = 1$; then the symmetric point of ψ is $\psi^* = 1/\bar{\psi}$. This means that points ψ and ψ^* have the same argument and are situated on the same half-line from the origin, and if one of the points is out of the circle, the second one is inside the circle, and vice versa. Hence, the points $\psi = 0$ and $\psi^* = \infty$ are symmetric points with respect to the circle.

The cross product (9) is invariant under the Möbius transformation; therefore if a Möbius transformation carries a generalized circle C_1 into a circle C_2, it transforms any pair of symmetric points with respect to C_1 into a pair of symmetric points with respect to C_2. According to this, if one considers the Möbius transformation, mapping the unit circle to the imaginary axis regarded as the generalized circle,

$$\psi_H = \frac{1 - \psi}{1 + \psi}, \tag{10}$$

then the symmetric point to the complex number ψ_H is just the reflection in the imaginary axis: $-\bar{\psi}_H$. For the Möbius transformation

$$\psi_H = \mathrm{i}\frac{1 - \psi}{1 + \psi}, \tag{11}$$

mapping the unit circle to the real axis, the symmetric point to ψ_H is $\bar{\psi}_H$. The composition of symmetric points in the real axis, $\psi \to \bar{\psi}$, in the imaginary axis, $\bar{\psi} \to -\psi$, and then in the unit circle, $-\psi \to -\frac{1}{\bar{\psi}}$, produces the negative-symmetric point $\psi^* = -\frac{1}{\bar{\psi}}$. The above-mentioned symmetric points have a simple geometrical meaning on the Bloch sphere:

1. ψ and $\psi^* = \bar{\psi}$ are projections of the points $M(x, y, z)$ and $M^*(x, -y, z)$.
2. ψ and $\psi^* = -\bar{\psi}$ are projections of the points $M(x, y, z)$ and $M^*(-x, y, z)$.
3. ψ and $\psi^* = \frac{1}{\bar{\psi}}$ are projections of the points $M(x, y, z)$ and $M^*(x, y, -z)$.
4. ψ and $\psi^* = -\frac{1}{\bar{\psi}}$ are projections of the points $M(x, y, z)$ and $M^*(-x, -y, -z)$.

The last case, corresponding to the antipodal points on the Bloch sphere, we study in detail in section 3. Here we would like to just note that the above four reflections for the symmetric points determine the anti-automorphisms considered in [14].

2.3. Symmetric qubits

Symmetric points are important in hydrodynamics theory and are related to the so-called method of images [18]. For the point vortex in the plane bounded by the cylindrical domain [18, 19] or

the annular domain (canonical region for the two-cylinder problem) [20], the symmetric points represent images of the vortex. Now we wish to introduce the coherent states corresponding to symmetric points and representing a symmetric pair of qubit states with remarkable properties. Then, we can interpret these quantum states as a qubit and its image state, realizing some kind of method of images in the quantum theory.

For a given qubit

$$|\theta, \varphi\rangle = \cos\frac{\theta}{2}|0\rangle + \sin\frac{\theta}{2}e^{i\varphi}|1\rangle = \begin{pmatrix} \cos\frac{\theta}{2} \\ \sin\frac{\theta}{2}\, e^{i\varphi} \end{pmatrix}, \tag{12}$$

in case 1, we have the symmetric qubit as

$$|\theta, -\varphi\rangle = \cos\frac{\theta}{2}|0\rangle + \sin\frac{\theta}{2}e^{-i\varphi}|1\rangle = \begin{pmatrix} \cos\frac{\theta}{2} \\ \sin\frac{\theta}{2}\, e^{-i\varphi} \end{pmatrix}, \tag{13}$$

and in case 2, it is

$$|\theta, \pi - \varphi\rangle = \cos\frac{\theta}{2}|0\rangle - \sin\frac{\theta}{2}e^{-i\varphi}|1\rangle = \begin{pmatrix} \cos\frac{\theta}{2} \\ -\sin\frac{\theta}{2}\, e^{-i\varphi} \end{pmatrix}. \tag{14}$$

Since the unit circle in the ψ plane, $|\psi|^2 = 1$, represents the equator on the Bloch sphere, then any point on the upper hemisphere projects to the external part of the unit circle, while on the lower hemisphere it is projected to the internal part of the circle. It is easy to see that if the point $M(x, y, z)$ is projected to ψ and then reflected in the equator, point $M^*(x, y, -z)$ is projected to the symmetric point ψ^*. According to this, we have the 'symmetric' qubit state in case 3 as

$$|\pi - \theta, \varphi\rangle = \sin\frac{\theta}{2}|0\rangle + \cos\frac{\theta}{2}e^{i\varphi}|1\rangle = \begin{pmatrix} \sin\frac{\theta}{2} \\ \cos\frac{\theta}{2}\, e^{i\varphi} \end{pmatrix}. \tag{15}$$

The above-mentioned pairs of qubit states define the symmetric qubit coherent states. The corresponding points M and M^* on the Bloch sphere are mirror images of each other in the coordinate planes xz, yz and xy, respectively. That is why we can call symmetrical qubit states (13)–(15) the mirror image qubits. For every complex number ψ as a projection of the point (θ, φ), we associate the coherent state (5). Then every point symmetric to ψ determines the symmetric coherent state. For the symmetric point $\psi^* = \bar{\psi}$, it is

$$|\bar{\psi}\rangle = \frac{|0\rangle + \bar{\psi}|1\rangle}{\sqrt{1 + |\psi|^2}}, \tag{16}$$

for the point $\psi^* = -\bar{\psi}$,

$$|-\bar{\psi}\rangle = \frac{|0\rangle - \bar{\psi}|1\rangle}{\sqrt{1 + |\psi|^2}}, \tag{17}$$

and for $\psi^* = \frac{1}{\bar{\psi}}$, the symmetric coherent state is

$$|\psi^*\rangle = |\frac{1}{\bar{\psi}}\rangle = \frac{\bar{\psi}|0\rangle + |1\rangle}{\sqrt{1 + |\psi|^2}}. \tag{18}$$

The limiting case of symmetric points $\psi = 0$ and $\psi^* = \infty$ in the first two cases reduces to the computational basis. In the third case, it gives the reversed basis $|\psi = 0\rangle = |1\rangle$, $|\psi^* = \infty\rangle = |0\rangle$. If one is dealing with the one-qubit gate represented by the linear transformation (2), the

corresponding Möbius transformation (1) transforms the unit circle at the origin to a generalized circle, so that symmetric points in the first circle transform to symmetric points with respect to the new one. This will define the transformation rule for symmetric qubit states. So the Möbius gate transforms the pair of symmetric qubits to the pair of symmetric qubits. In the following sections, we find Möbius transformations related to basic quantum gates.

3. Antipodal symmetric coherent states

3.1. Generalized coherent state basis

As we have seen in the previous section, the computational basis can be considered as a specific case of symmetric coherent states. Then, the expansion of an arbitrary qubit state in the computational basis $|\phi\rangle = c_1|0\rangle + c_2|1\rangle$ is an expansion to particular symmetric coherent states. It suggests a natural generalization of this expansion to arbitrary symmetrical states (16)–(18)

$$|\phi\rangle = d_1|\psi\rangle + d_2|\psi^*\rangle, \tag{19}$$

with the $|\psi\rangle$ and $|\psi^*\rangle$ states as a basis. However, this basis is not orthonormal. Due to (18)

$$\langle\psi^*|\psi\rangle = \frac{2|\psi|}{1+|\psi|^2} \leqslant 1, \tag{20}$$

$$d_1 = \langle\psi|\phi\rangle = \frac{c_1 + \bar{\psi}c_2}{\sqrt{1+|\psi|^2}}, \quad d_2 = \langle\psi^*|\phi\rangle = \frac{|\psi_1|c_1 + \frac{|\psi|}{\psi}c_2}{\sqrt{1+|\psi|^2}}, \tag{21}$$

and we have

$$|\phi\rangle = \frac{c_1 + \bar{\psi}c_2}{\sqrt{1+|\psi|^2}}|\psi\rangle + \frac{|\psi_1|c_1 + \frac{|\psi|}{\psi}c_2}{\sqrt{1+|\psi|^2}}|\psi^*\rangle. \tag{22}$$

It becomes orthonormal only in the case of computational basis, when $\psi \to 0$ or $\psi \to \infty$. In the particular case when ψ belongs to the unit circle $|\psi| = 1$, the symmetric points coincide $\psi = \psi^*$, so that $\langle\psi^*|\psi\rangle = \langle\psi|\psi^*\rangle = 1$ and we have just the one state.

3.1.1. Antipodal qubit and negative-symmetric basis. The above-introduced states $|\psi\rangle$ and $|\psi^*\rangle$ in (16)–(18) are not orthogonal. To have the orthogonal state for a given state $|\psi\rangle$, we consider the negative-symmetric state $|-\psi^*\rangle$ from case 4. This state is represented by the point $-\psi^* = -1/\bar{\psi}$, which is a rotation of the symmetric point $\psi^* = 1/\bar{\psi}$ through angle π. We call this point the negative-symmetric point or the inverse mirror image, and the corresponding coherent state the negative-symmetric coherent state (inverse mirror image state). Point $M(x, y, z)$, representing the qubit state $|\theta, \varphi\rangle$ on the Bloch sphere, gives the antipodal point $M^*(-x, -y, -z)$ and the corresponding state

$$|\pi - \theta, \varphi + \pi\rangle = \sin\frac{\theta}{2}|0\rangle - \cos\frac{\theta}{2}e^{i\varphi}|1\rangle = \begin{pmatrix} \sin\frac{\theta}{2} \\ -\cos\frac{\theta}{2}e^{i\varphi} \end{pmatrix}, \tag{23}$$

which we call the antipodal qubit state. For the state (5) we have explicitly

$$|-\psi^*\rangle = \frac{|0\rangle - \psi^*|1\rangle}{\sqrt{1+|\psi^*|^2}} = \frac{|\psi||0\rangle - \frac{|\psi|}{\bar{\psi}}|1\rangle}{\sqrt{1+|\psi|^2}}. \tag{24}$$

This state, up to the global phase, can be rewritten in the form

$$|-\psi^*\rangle = \frac{-\bar{\psi}|0\rangle + |1\rangle}{\sqrt{1+|\psi|^2}}. \tag{25}$$

In contrast to the symmetric state (18), the negative-symmetric state (25) is orthogonal to $|\psi\rangle$:

$$\langle -\psi^*|\psi\rangle = 0. \tag{26}$$

In addition, the states $|\psi\rangle$ and $|-\psi^*\rangle$ satisfy the completeness relation

$$|\psi\rangle\langle\psi| + |-\psi^*\rangle\langle-\psi^*| = I \tag{27}$$

and form the orthonormal basis, so that for any state

$$|\phi\rangle = e_1|\psi\rangle + e_2|-\psi^*\rangle \tag{28}$$

we have

$$e_1 = \langle\psi|\phi\rangle = \frac{c_1 + c_2\bar{\psi}}{\sqrt{1+|\psi|^2}}, \quad e_2 = \langle -\psi^*|\phi\rangle = \frac{-\psi c_1 + c_2}{\sqrt{1+|\psi|^2}}. \tag{29}$$

As is well known, the set of spin-coherent states is the overcomplete set [3]. By using the 'resolution of unity'

$$\int \mathrm{d}\mu(\psi)|\psi\rangle\langle\psi| = I, \tag{30}$$

where

$$\mathrm{d}\mu(\psi) = \frac{2}{\pi}\frac{\mathrm{d}^2\psi}{(1+|\psi|^2)^2} \tag{31}$$

is an arbitrary state that can be decomposed over the coherent states

$$|\Phi\rangle = \int \mathrm{d}\mu(\psi)\Phi(\bar{\psi})|\psi\rangle. \tag{32}$$

Then, our relations (26) and (27) show that two orthogonal states $|\psi\rangle$ and $|-\psi^*\rangle$ give a subsystem of complete orthogonal states and the dimension of our Hilbert space is two.

3.1.2. Antipodal coherent state for arbitrary representation j. The antipodal states can be derived also for spin j representation of $su(2)$ Lie algebra:

$$[S_3, S_+] = S_+, \quad [S_3, S_-] = -S_-, \quad [S_+, S_-] = 2S_3, \tag{33}$$

where $S_\pm = \frac{1}{2}(S_1 \pm \mathrm{i}S_2)$, so that

$$S_+|j, m\rangle = \sqrt{(j-m)(j+m+1)}|j, m+1\rangle, \tag{34}$$

$$S_-|j, m\rangle = \sqrt{(j-m+1)(j+m)}|j, m-1\rangle, \tag{35}$$

$$S_3|j, m\rangle = m|j, m\rangle, \tag{36}$$

where $-j \leqslant m \leqslant j$. The coherent state $|\psi\rangle$, $\psi \in C$, is defined as

$$|\psi\rangle = \frac{1}{(1+|\psi|^2)^j}\sum_{k=0}^{2j}\left(\frac{(2j)!}{k!(2j-k)!}\right)^{1/2}\psi^k\ |j, -j+k\rangle. \tag{37}$$

For the scalar product of two coherent states, after simple calculations we have

$$\langle\phi|\psi\rangle = \frac{(1+\bar{\phi}\,\psi)^{2j}}{(1+|\phi|^2)^j(1+|\psi|^2)^j}. \tag{38}$$

Then, the orthogonality condition implies $1+\bar{\phi}\,\psi = 0$ or the negative-symmetric point in the unit circle $\phi = -\frac{1}{\bar{\psi}}$. The representation of these coherent states in terms of the unit vector $\mathbf{n}$

$$\langle\mathbf{n}_1|\mathbf{n}_2\rangle = \mathrm{e}^{\mathrm{i}\theta(\mathbf{n}_1,\mathbf{n}_2)}\left(\frac{1+\mathbf{n}_1\mathbf{n}_2}{2}\right)^j \tag{39}$$

shows that the above points are antipodal points on the Bloch sphere $\mathbf{n}_1\mathbf{n}_2 = -1$.

The resolution of unity in this case is [17]

$$\int \mathrm{d}\mu_j(\psi)|\psi\rangle\langle\psi| = I, \tag{40}$$

where

$$\mathrm{d}\mu_j(\psi) = \frac{2j+1}{\pi}\frac{\mathrm{d}^2\psi}{(1+|\psi|^2)^2}. \tag{41}$$

Then, an arbitrary state can be decomposed over the coherent states as

$$|\Phi\rangle = \int \mathrm{d}\mu_j(\psi)\Phi(\bar{\psi})|\psi\rangle, \tag{42}$$

where

$$\Phi(\bar{\psi}) = \langle\psi|\Phi\rangle = \frac{1}{(1+|\psi|^2)^j}\sum_{k=-j}^{j} c_k\left(\frac{(2j)!}{(j+k)!(j-k)!}\right)^{1/2}\bar{\psi}^{\,j+k} \tag{43}$$

and the function in the numerator is just a polynomial of $\bar{\psi}$ of an order $m \leqslant 2j$. As a result, to any complex function $f(\psi) = P_m(\psi)/(1+|\psi|^2)^j$, where $P_m(\psi)$ is an arbitrary polynomial of degree $m \leqslant 2j$, corresponds a state vector $|\Phi\rangle$ given by

$$f(\psi) = \langle\Phi|\psi\rangle, \qquad \int \mathrm{d}\mu_j(\psi)\langle\xi|\psi\rangle f(\psi) = f(\xi). \tag{44}$$

The set of such functions is the Hilbert space, describing states of a spin-j system. The dimension of this space is $2j+1$, and the subset of the states determined by an arbitrary choice of nonequal points $\psi_1, \psi_2, \ldots, \psi_{2j+1}$ is complete. It follows from the observation that any polynomial of degree $2j$ is determined completely by its values at $2j+1$ points. For $j = 1/2$ we have the 2D Hilbert space with two orthogonal states $|\psi\rangle$ and $|-\psi^*\rangle$, constituting the basis (27).

3.2. Unitary Möbius transformation

From the set of fractional linear transformations (1), determined by an arbitrary $SL(2, C)$ matrix (2), for quantum computations there is an important class of unitary transformations given by the matrix

$$U = \begin{pmatrix} a & b \\ -\bar{b} & \bar{a} \end{pmatrix}, \tag{45}$$

where $|a|^2+|b|^2=1$. Acting on a qubit state $|\psi\rangle=\psi_1|0\rangle+\psi_2|1\rangle$, it implies the Möbius transformation

$$\psi_U=\frac{a\psi+b}{-\bar{b}\psi+\bar{a}} \tag{46}$$

for $\psi=\psi_1/\psi_2$, and the linear transformation

$$|\psi_U\rangle=\left|\frac{a\psi+b}{-\bar{b}\psi+\bar{a}}\right\rangle=U|\psi\rangle, \tag{47}$$

acting, up to the phase, on the coherent state

$$|\psi\rangle=\frac{1}{\sqrt{1+|\psi|^2}}\begin{pmatrix}\psi\\1\end{pmatrix}. \tag{48}$$

This state differs from state (5) by the flipping transformation. The NOT gate $\sigma_1=X\equiv\mathrm{NOT}$ acts on a qubit state $|\psi\rangle=\psi_1|0\rangle+\psi_2|1\rangle$ as flipping

$$|\psi_{\mathrm{NOT}}\rangle=\sigma_1|\psi\rangle=\psi_2|0\rangle+\psi_1|1\rangle, \tag{49}$$

and implies the Möbius transformation $\psi\to\psi_{\mathrm{NOT}}=\frac{1}{\psi}$, connecting (up to the phase) two coherent states (5) and (48):

$$|\psi_{\mathrm{NOT}}\rangle=\frac{1}{\sqrt{1+|\psi_{\mathrm{NOT}}|^2}}\begin{pmatrix}\psi_{\mathrm{NOT}}\\1\end{pmatrix}=\frac{1}{\sqrt{1+|\psi|^2}}\begin{pmatrix}1\\\psi\end{pmatrix}. \tag{50}$$

Due to this we denote the flipped state (48) as $|\psi_{\mathrm{NOT}}\rangle$. Now we consider universal gates such as the Hadamard gate and the phase gate.

1. The Hadamard gate

$$H=\frac{1}{\sqrt{2}}\begin{pmatrix}1&1\\1&-1\end{pmatrix} \tag{51}$$

acts on coherent state (5) as

$$|\psi_H\rangle=H|\psi\rangle=\frac{1}{\sqrt{1+|\psi|^2}}\begin{pmatrix}1+\psi\\1-\psi\end{pmatrix}=\frac{1}{\sqrt{1+|\psi_H|^2}}\begin{pmatrix}1\\\psi_H\end{pmatrix}, \tag{52}$$

and implies the Möbius transformation

$$\psi_H=\frac{1-\psi}{1+\psi}. \tag{53}$$

On state (18) it acts as

$$|\psi_H^*\rangle=H|\psi^*\rangle=\frac{1}{\sqrt{1+|\psi^*|^2}}\begin{pmatrix}1+\psi^*\\1-\psi^*\end{pmatrix}=\frac{1}{\sqrt{1+|\psi_H^*|^2}}\begin{pmatrix}1\\v\psi_H^*\end{pmatrix} \tag{54}$$

where

$$\psi_H^*=\frac{1-\psi^*}{1+\psi^*}=\frac{\bar{\psi}-1}{\bar{\psi}+1}. \tag{55}$$

Under this fractional transformation, the unit circle $|\psi|^2=1$ transforms to the imaginary axis in the ψ plane: $\psi_H=\mathrm{i}\Im\psi_H$, and images of symmetric points ψ_H and ψ_H^* are

symmetric with respect to this axis. The corresponding symmetric states $|\psi_H\rangle$ and $|\psi_H^*\rangle$ are disposed on the Bloch sphere, equidistantly from the vertical plane through $\Re\psi = 0$. For the negative-symmetric point, we obtain the transformation

$$(-\psi^*)_H = \frac{1+\psi^*}{1-\psi^*} = \frac{\bar{\psi}+1}{\bar{\psi}-1} = -\frac{1}{\bar{\psi}_H}. \tag{56}$$

This formula means that points ψ_H and $(-\psi^*)_H$ are the negative-symmetric points, but now with respect to the unit circle at the origin. Hence, we found that the Hadamard gate transforms symmetric points with respect to the unit circle into symmetric points with respect to the imaginary axis, and negative-symmetric points into negative-symmetric points, but with respect to the unit circle.

2. For the phase shift gate

$$R_z(\theta) = \begin{pmatrix} 1 & 0 \\ 0 & \mathrm{e}^{\mathrm{i}\theta} \end{pmatrix} \tag{57}$$

we have the transformation

$$|\psi_R\rangle = R_z(\theta)|\psi\rangle = \frac{1}{\sqrt{1+|\psi|^2}}\begin{pmatrix} 1 \\ \mathrm{e}^{\mathrm{i}\theta}\psi \end{pmatrix} = \frac{1}{\sqrt{1+|\psi_R|^2}}\begin{pmatrix} 1 \\ \psi_R \end{pmatrix}, \tag{58}$$

which implies rotation around the origin through angle $\theta : \psi_R = \mathrm{e}^{\mathrm{i}\theta}\psi$. The same rotation acts on the symmetric and the negative-symmetric points.

3.2.1. Coherent Hadamard basis. The Hadamard basis $H|0\rangle = \frac{1}{\sqrt{2}}(|0\rangle + |1\rangle) \equiv |+\rangle$ and $H|1\rangle = \frac{1}{\sqrt{2}}(|0\rangle - |1\rangle) \equiv |-\rangle$, under the action $U|0\rangle = |\psi\rangle$ and $U|1\rangle = |-\psi^*\rangle$, transforms into

$$U|+\rangle = \frac{1}{\sqrt{2}}(|\psi\rangle + |-\psi^*\rangle) \equiv |\psi_+\rangle, \tag{59}$$

$$U|-\rangle = \frac{1}{\sqrt{2}}(|\psi\rangle - |-\psi^*\rangle) \equiv |\psi_-\rangle. \tag{60}$$

This coherent state Hadamard basis is generated from our coherent states by the unitary transformation

$$|\psi_+\rangle = (UHU^{-1})|\psi\rangle, \tag{61}$$

$$|\psi_-\rangle = (UHU^{-1})|-\psi^*\rangle. \tag{62}$$

4. The two-qubit case

4.1. Coherent state orthonormal basis

Here we consider the generic two-qubit coherent state

$$|\psi_1\rangle|\psi_2\rangle = \frac{1}{\sqrt{1+|\psi_1|^2}\sqrt{1+|\psi_2|^2}}\begin{pmatrix} 1 & \psi_2 & \psi_1 & \psi_1\psi_2 \end{pmatrix}^{\mathrm{T}}. \tag{63}$$

By proper choice of ψ_1 and ψ_2 we can construct the two-qubit orthonormal coherent state basis. We find this basis in the following form:

$$|\psi\rangle|\psi\rangle = \frac{1}{1+|\psi|^2}\begin{pmatrix}1 & \psi & \psi & \psi^2\end{pmatrix}^{\mathrm{T}}, \tag{64}$$

$$|\psi\rangle|-\psi^*\rangle = \frac{1}{1+|\psi|^2}\begin{pmatrix}-\bar{\psi} & 1 & -|\psi|^2 & \psi\end{pmatrix}^{\mathrm{T}}, \tag{65}$$

$$|-\psi^*\rangle|\psi\rangle = \frac{1}{1+|\psi|^2}\begin{pmatrix}-\bar{\psi} & -|\psi|^2 & 1 & \psi\end{pmatrix}^{\mathrm{T}}, \tag{66}$$

$$|-\psi^*\rangle|-\psi^*\rangle = \frac{1}{1+|\psi|^2}\begin{pmatrix}\bar{\psi}^2 & -\bar{\psi} & -\bar{\psi} & 1\end{pmatrix}^{\mathrm{T}}, \tag{67}$$

as the orthonormal coherent state basis. These states can be generated from the computational basis by the operator

$$U = \frac{1}{\sqrt{1+|\psi|^2}}\begin{pmatrix}1 & -\bar{\psi}\\ \psi & 1\end{pmatrix}, \tag{68}$$

so that

$$|\psi\rangle|\psi\rangle = (U\otimes U)|00\rangle = \hat{U}_{12}|00\rangle, \tag{69}$$

$$|\psi\rangle|-\psi^*\rangle = (U\otimes U)|01\rangle = \hat{U}_{12}|01\rangle, \tag{70}$$

$$|-\psi^*\rangle|\psi\rangle = (U\otimes U)|10\rangle = \hat{U}_{12}|10\rangle, \tag{71}$$

$$|-\psi^*\rangle|-\psi^*\rangle = (U\otimes U)|11\rangle = \hat{U}_{12}|11\rangle, \tag{72}$$

where $\hat{U}_{12} = U\otimes U$.

4.1.1. Generation of maximally entangled states from coherent state basis. Due to separability, these states are not entangled, nor is the computational basis. However, we can generate the maximally entangled Bell states from the computational basis by using a combination of the Hadamard gate and the CNOT gate: the Hadamard gate applied to the left qubit, followed by the CNOT gate C : CNOT$(H\otimes I)$:

$$C|00\rangle = |\phi_B^+\rangle = \frac{1}{\sqrt{2}}(|00\rangle+|11\rangle),\ C|01\rangle = |\psi_B^+\rangle = \frac{1}{\sqrt{2}}(|01\rangle+|10\rangle), \tag{73}$$

$$C|10\rangle = |\phi_B^-\rangle = \frac{1}{\sqrt{2}}(|00\rangle-|11\rangle),\ C|11\rangle = |\psi_B^-\rangle = \frac{1}{\sqrt{2}}(|01\rangle-|10\rangle). \tag{74}$$

This allows us to introduce the next set of coherent states

$$|P_+\rangle = (\hat{U}_{12}C\hat{U}_{12}^{-1})|\psi\psi\rangle = \hat{U}_{12}C(\hat{U}_{12}^{-1}\hat{U}_{12})|00\rangle = \hat{U}_{12}|\phi_B^+\rangle, \tag{75}$$

$$|P_-\rangle = (\hat{U}_{12}C\hat{U}_{12}^{-1})|\psi\,-\psi^*\rangle = \hat{U}_{12}C(\hat{U}_{12}^{-1}\hat{U}_{12})|01\rangle = \hat{U}_{12}|\phi_B^-\rangle, \tag{76}$$

$$|G_+\rangle = (\hat{U}_{12}C\hat{U}_{12}^{-1})|-\psi^*\psi\rangle = \hat{U}_{12}C(\hat{U}_{12}^{-1}\hat{U}_{12})|10\rangle = \hat{U}_{12}|\psi_B^+\rangle, \tag{77}$$

$$|G_-\rangle = (\hat{U}_{12}C\hat{U}_{12}^{-1})|-\psi^*\,-\psi^*\rangle = \hat{U}_{12}C(\hat{U}_{12}^{-1}\hat{U}_{12})|11\rangle = \hat{U}_{12}|\psi_B^-\rangle. \tag{78}$$

The set $|P_\pm\rangle$, $|G_\pm\rangle$ is an orthonormal set of two-qubit coherent states and for particular values $\psi \to 0$ and $\psi \to \infty$, it reduces to the Bell basis. This is also a complete set, satisfying the resolution of unity

$$|P_+\rangle\langle P_+| + |P_-\rangle\langle P_-| + |G_+\rangle\langle G_+| + |G_-\rangle\langle G_-| = I, \tag{79}$$

which is easy to prove from explicit representation (98) and (99). Thus, any two-qubit state can be expanded in this set as a basis. The concurrence formula for a two-qubit state, expanded in the Bell basis

$$|\phi\rangle = s^+|\phi_+\rangle + s^-|\phi_-\rangle + h^+|\psi_+\rangle + h^-|\psi_-\rangle, \tag{80}$$

is given by

$$C = |s^{+2} - s^{-2} - h^{+2} + h^{-2}|. \tag{81}$$

Then, we find a similar formula for the state $|\psi\rangle$ expanded according to our basis

$$|\phi\rangle = b^+|P_+\rangle + b^-|P_-\rangle + c^+|G_+\rangle + c^-|G_-\rangle, \tag{82}$$

so that the concurrence becomes

$$C = |b^{+2} - b^{-2} - c^{+2} + c^{-2}|. \tag{83}$$

5. Maximally entangled orthogonal two-qubit coherent states

Here we show that the set of states (75)–(78)

$$|P_\pm\rangle = \frac{1}{\sqrt{2}}(|\psi\rangle|\psi\rangle \pm |-\psi^*\rangle|-\psi^*\rangle), \tag{84}$$

$$|G_\pm\rangle = \frac{1}{\sqrt{2}}(|\psi\rangle|-\psi^*\rangle \pm |-\psi^*\rangle|\psi\rangle) \tag{85}$$

is a maximally entangled set of orthogonal two-qubit states. To show this, we follow three different methods, the reduced density matrix method, the determinant method and the vanishing of the average of dynamical variables method for maximally non-classical states. Since the dimension of the Hilbert space for our pure states is four, these methods are sufficient to establish maximal entanglement of our states.

First we follow the reduced density matrix approach. The density matrix for the pure states $|P_\pm\rangle$ in the coherent state basis is

$$\rho_P^\pm = |P_\pm\rangle\langle P_\pm| \tag{86}$$

$$= \tfrac{1}{2}(|\psi\rangle|\psi\rangle\langle\psi|\langle\psi| \pm |\psi\rangle|\psi\rangle\langle-\psi^*|\langle-\psi^*| \tag{87}$$

$$\pm |-\psi^*\rangle|-\psi^*\rangle\langle\psi|\langle\psi| + |-\psi^*\rangle|-\psi^*\rangle\langle-\psi^*|\langle-\psi^*|). \tag{88}$$

The reduced density matrix at Bob's site can be written as

$$\rho_B^\pm = \mathrm{tr}_B\,(\rho_P^\pm) = \langle\psi|\rho_P^\pm|\psi\rangle + \langle-\psi^*|\rho_P^\pm|-\psi^*\rangle \tag{89}$$

$$= \tfrac{1}{2}(|\psi\rangle\langle\psi| + |-\psi^*\rangle\langle-\psi^*|) \tag{90}$$

$$= \frac{1}{2}\begin{pmatrix} 1 & 0 \\ 0 & 1 \end{pmatrix}, \tag{91}$$

so that $\mathrm{tr}(\rho_B^{\pm}) = 1$ and $\mathrm{tr}(\rho_B^{\pm})^2 = \frac{1}{2}$. Hence, the reduced density operator $\rho_B^{\pm}$ represents a mixed state. Since the concurrence in this state is $C = \sqrt{2(1 - \mathrm{tr}\rho_B^2)} = 1$, we conclude that $|P_{\pm}\rangle$ are the maximally entangled states. In a similar way, we can show that $|G_{\pm}\rangle$ are also the maximally entangled states. Indeed, the density matrix for the pure states $|G_{\pm}\rangle$ in the coherent state basis

$$\rho_G^{\pm} = |G_{\pm}\rangle\langle G_{\pm}| \tag{92}$$

$$= \tfrac{1}{2}(|\psi\rangle|-\psi^*\rangle\langle\psi|\langle-\psi^*| \pm |\psi\rangle|-\psi^*\rangle\langle-\psi^*|\langle\psi| \tag{93}$$

$$\pm |-\psi^*\rangle|\psi\rangle\langle\psi|\langle-\psi^*| + |-\psi^*\rangle|\psi\rangle\langle-\psi^*|\langle\psi|) \tag{94}$$

gives the reduced density matrix

$$\rho_B^{\pm} = \mathrm{tr}_B\,(\rho_G^{\pm}) = \langle\psi|\rho_G^{\pm}|\psi\rangle + \langle-\psi^*|\rho_G^{\pm}|-\psi^*\rangle \tag{95}$$

$$= \tfrac{1}{2}(|\psi\rangle\langle\psi| + |-\psi^*\rangle\langle-\psi^*|) \tag{96}$$

$$= \frac{1}{2}\begin{pmatrix} 1 & 0 \\ 0 & 1 \end{pmatrix}, \tag{97}$$

so that $\mathrm{tr}(\rho_B^{\pm}) = 1$ and $\mathrm{tr}(\rho_B^{\pm})^2 = \frac{1}{2}$, and the state is mixed. From the concurrence $C = \sqrt{2(1-\rho_B^2)} = 1$, it then follows that $|G_{\pm}\rangle$ are the maximally entangled states.

Explicitly for these states we have

$$|P_+\rangle = \frac{1}{\sqrt{2}(1+|\psi|^2)}\begin{pmatrix} 1+\bar{\psi}^2 \\ \psi-\bar{\psi} \\ \psi-\bar{\psi} \\ 1+\psi^2 \end{pmatrix}, \quad |P_-\rangle = \frac{1}{\sqrt{2}(1+|\psi|^2)}\begin{pmatrix} 1-\bar{\psi}^2 \\ \psi+\bar{\psi} \\ \psi+\bar{\psi} \\ -1+\psi^2 \end{pmatrix}, \tag{98}$$

$$|G_+\rangle = \frac{1}{\sqrt{2}(1+|\psi|^2)}\begin{pmatrix} -2\bar{\psi} \\ 1-|\psi|^2 \\ 1-|\psi|^2 \\ 2\psi \end{pmatrix}, \quad |G_-\rangle = \frac{1}{\sqrt{2}(1+|\psi|^2)}\begin{pmatrix} 0 \\ 1+|\psi|^2 \\ -1-|\psi|^2 \\ 0 \end{pmatrix}. \tag{99}$$

This form is convenient to calculate the concurrence for a pure state $|\Phi\rangle$ in the determinant form

$$C_{12} = 2\begin{vmatrix} t_{00} & t_{01} \\ t_{10} & t_{11} \end{vmatrix} = 2|t_{00}t_{11} - t_{01}t_{10}|, \tag{100}$$

where $t_{ij}(i, j = 0, 1)$ are the coefficients of expansion for this state in the computational basis

$$|\Phi\rangle = t_{00}|00\rangle + t_{01}|01\rangle + t_{10}|10\rangle + t_{11}|11\rangle. \tag{101}$$

Applying this definition to states (98) and (99), we find that concurrence $C_{12} = 1$, as we expected.

Finally, if we add two spins

$$\hat{\vec{S}}_{\pm} = \hat{\vec{S}}_1 \otimes I \pm I \otimes \hat{\vec{S}}_2 \tag{102}$$

and calculate their averages in our states (84) and (85), then we find that they vanish:

$$\langle P_\pm|\hat{S}^z_\pm|P_\pm\rangle = 0, \quad \langle P_\pm|\hat{S}^+_\pm|P_\pm\rangle = 0, \tag{103}$$

$$\langle G_\pm|\hat{S}^z_\pm|G_\pm\rangle = 0, \quad \langle G_\pm|\hat{S}^+_\pm|G_\pm\rangle = 0. \tag{104}$$

This property has been used in [21] as an operational definition of completely entangled states, which are considered as maximally non-classical states. Therefore, this also confirms that our states are maximally entangled states.

At first glance, since our states are continuous-variable states, the quantification of entanglement for these non-Gaussian states needs to be clarified. This is due to the fact that only the Gaussian states have been completely characterized for the case of continuous-variables. However, although our states are defined in a high-dimensional Hilbert space, they have small Schmidt rank, namely 2, which is shown above by computing the reduced density operator at Bob's site. Thus, these states can local-unitarily be mapped to a two-qubit Hilbert space and their entanglement properties are thus no different from those of the two-qubit case. It justifies our use of the concurrence in this section. This approach is also valid for arbitrary spin-coherent states of a spin j, living in $(2j+1)$-dimensional Hilbert space, so that two-qubit states belong to $H = C^{2j+1} \times C^{2j+1}$. By using the Holstein–Primakoff representation, mapping spin operators to the boson creation and annihilation operators, we find for large j the spin-coherent states approach the bosonic coherent states. So, it makes sense to embed the states in the infinite-dimensional Hilbert space by identifying $|j, m-j\rangle$ with the Fock state $|m\rangle$. Then, one could try to characterize these states by 'continuous-variables', e.g. the operators X, P and their covariances. But since the Schmidt rank of our states is 2, we do not think that one would learn much about the state from a continuous-variable perspective and would rather say that it is locally unitarily equivalent to a two-qubit state. Then, we just recall that all pure state entanglement properties are fully captured by the Schmidt coefficients of the state, which are $1/\sqrt{2}, 1/\sqrt{2}$ in our case. So our application of concurrence in this section seems perfectly correct.

6. Operators and their Q symbols

Using coherent states one may represent operators acting on the Hilbert space in terms of a certain class of functions, which determines the operators completely, and these are called operator symbols [17]. For the Glauber coherent states, the operator symbol $A(\bar{\alpha}, \beta) = \langle\alpha|A|\beta\rangle$ is an analytical function of complex variables $\bar{\alpha}$ and β and is determined completely by its diagonal values,

$$A(\bar{\alpha}, \alpha) = \langle\alpha|A|\alpha\rangle, \tag{105}$$

which are called Q symbols of operator A.

Operator symbols can be considered as functions on the phase space of a classical dynamical system. In this case, coherent states may provide the natural means for quantization and its classical correspondence. In the following, we consider the Hamiltonian operator H and its average $\langle\psi|H|\psi\rangle$ in our spin-coherent states as the Q symbol of H: $Q_H(\psi)$. As is well known, if an operator is bounded, then it always has a Q symbol [17], which is a value of an entire function $\mathcal{H}(\psi, \psi) = \langle\psi|H|\psi\rangle$. For the spin model with a finite number of qubits, the Hamiltonian is a bounded operator; that is why its symbol always exists and is representable

as a finite function. This function, the average energy in the coherent state, appears as a finite-energy configuration in the phase space of the system. Below we study the XYZ spin model for two- and three-qubit states, and calculate the Q symbol of H, as an average energy in the coherent state.

We would like to stress that our two-qubit coherent states are maximally entangled states and are determined by one complex ψ or two real parameters. These parameters can be fixed by concrete physical requirements on minimal energy, or some constraints on fidelity, etc, but will not change the entanglement of the system. That is why our Q symbol of the Hamiltonian appears as a localized finite energy in maximally entangled two (three or higher)-qubit phase space.

- First, we consider the XXX model,

$$H = -J(S_1^+ S_2^- + S_1^- S_2^+ + 2S_1^z S_2^z), \tag{106}$$

where $S_x = \frac{S^+ + S^-}{2}$, $S_y = \frac{S^+ - S^-}{2\mathrm{i}}$ and

$$S^+|0\rangle = 0, \quad S^+|1\rangle = \hbar|0\rangle, \tag{107}$$

$$S^-|0\rangle = \hbar|1\rangle, \quad S^-|1\rangle = 0, \tag{108}$$

$$S_z|0\rangle = \frac{\hbar}{2}|0\rangle, \quad S_z|1\rangle = -\frac{\hbar}{2}|1\rangle. \tag{109}$$

Then we find the Q symbol of this Hamiltonian in the $|P_+\rangle$ state just as a constant

$$\langle P_+|H|P_+\rangle = -\frac{J\hbar^2}{2}. \tag{110}$$

- For the XXZ model

$$H = -J(S_1^+ S_2^- + S_1^- S_2^+) + 2\Delta S_1^z S_2^z, \tag{111}$$

where $J\Delta = J_z$, we have

$$\langle P_+|H|P_+\rangle = \frac{-2\hbar^2}{(1+|\psi|^2)^2}\left[-J(\psi - \bar{\psi})^2 + J_z\left(\frac{(1-|\psi|^2)^2}{2} + \psi^2 + \bar{\psi}^2\right)\right], \tag{112}$$

and in terms of $\psi = x + \mathrm{i}y$,

$$\langle P_+|H|P_+\rangle = -\hbar^2 \frac{8Jy^2 + J_z[1 + 2x^2 - 6y^2 + (x^2+y^2)^2]}{(1+x^2+y^2)^2}. \tag{113}$$

In figure 1 we show the average energy surface $\langle P_+|H|P_+\rangle = E(x, y)$ as a function of x, y for $J = 1$, $J_z = -2$. It has two local minima at $(0, \pm 1)$.

6.1. Two-qubit energy in the XYZ model

Here we calculate the average energy for the XYZ model

$$H = \tfrac{1}{2}[J_x \sigma_1^x \sigma_2^x + J_y \sigma_1^y \sigma_2^y + J_z \sigma_1^z \sigma_2^z], \tag{114}$$

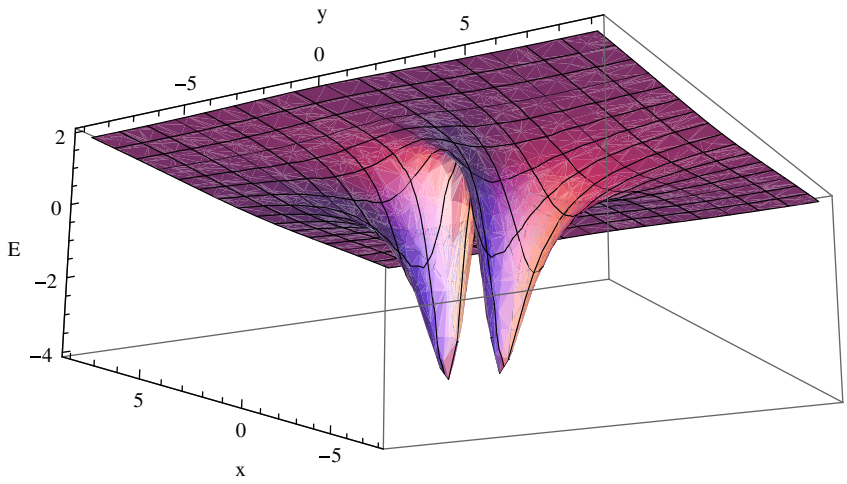

Figure 1. The average energy surface of the XXZ model in the maximally entangled state $|P_+\rangle$, $J = 1$ and $J_z = -2$.

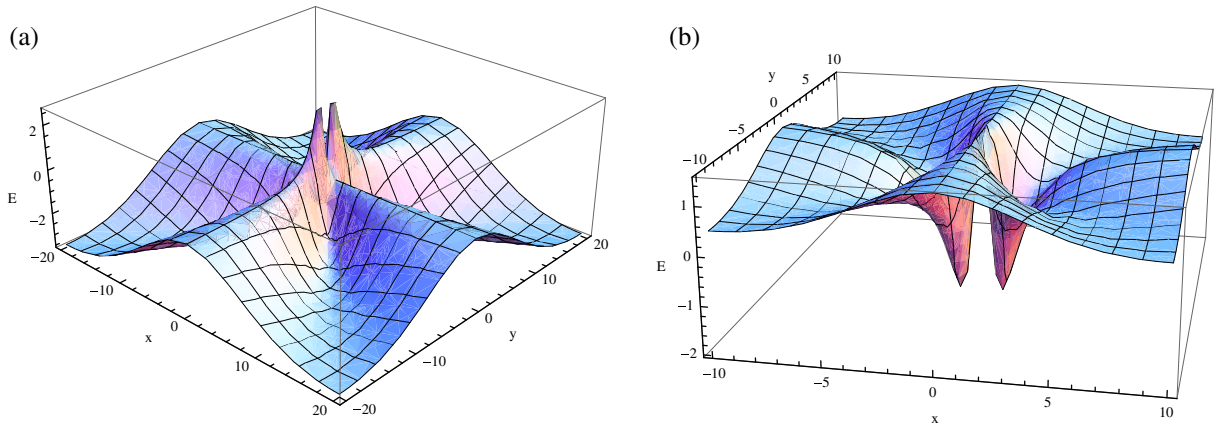

Figure 2. The average energy surface for the XYZ model in the maximally entangled state: (a) $|P_+\rangle$ for $J_+ = 1$, $J_- = 1.5$ and $J_z = -4$; (b) $|P_-\rangle$ for $J_+ = -1$, $J_- = -0.5$ and $J_z = 2$.

in two-qubit spin-coherent states (84) and (85). In the $|P_+\rangle$ state, we find ($\hbar = 1$)

$$\langle P_+|H|P_+\rangle = \frac{-2J_+(\psi - \bar{\psi})^2 + J_-[(1+\psi^2)^2 + (1+\bar{\psi}^2)^2] + J_z[(1-|\psi|^2)^2 + 2(\psi^2 + \bar{\psi}^2)]}{2(1+|\psi|^2)^2}. \tag{115}$$

In figure 2(a) we show the energy surface as a function of $x = \Re\psi$, $y = \Im\psi$, $J_+ = 1$, $J_- = 1.5$, $J_z = -4$, with characteristic local maxima at points $(0, \pm 1)$.

For the state $|P_-\rangle$ we have

$$\langle P_-|H|P_-\rangle = \frac{2J_+(\psi + \bar{\psi})^2 - J_-[(1-\psi^2)^2 + (1-\bar{\psi}^2)^2] + J_z[(1-\psi^2)(1-\bar{\psi}^2) - (\psi + \bar{\psi})^2]}{2(1+|\psi|^2)^2}. \tag{116}$$

It is shown in figure 2(b), for $J_+ = -1$, $J_- = -0.5$, $J_z = 2$, with two local minima at $(\pm 1, 0)$.

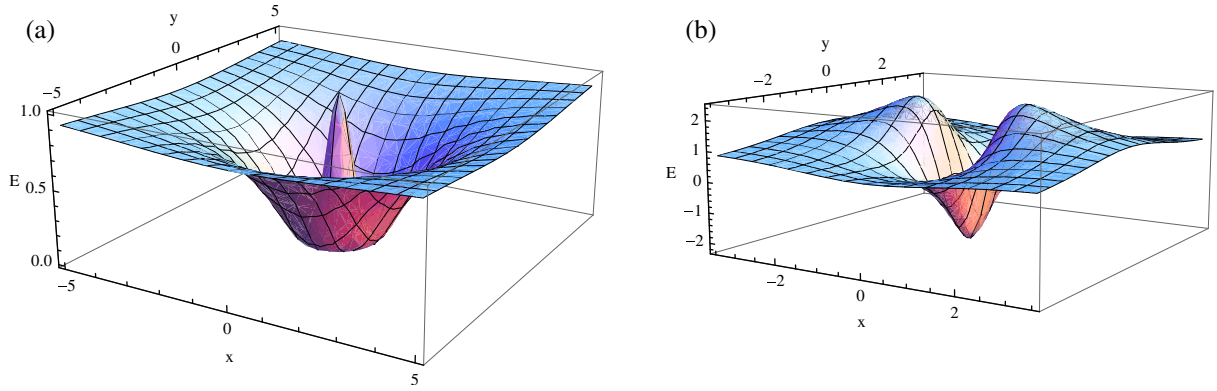

Figure 3. The average energy of the XYZ model in the maximally entangled state $|G_+\rangle$: (a) for $J_+ = 1$, $J_- = 0$ and $J_z = 0$; (b) for $J_+ = -1.5$, $J_- = -1.5$ and $J_z = 1.5$.

For the state $|G_+\rangle$ the average energy is

$$\langle G_+|H|G_+\rangle = \frac{2J_+(1-|\psi|^2)^2 - 4J_-[\psi^2+\bar{\psi}^2] + J_z[4|\psi|^2 - (1-|\psi|^2)^2]}{2(1+|\psi|^2)^2}. \tag{117}$$

In figure 3(a) we show the average energy surface for $J_+ = 1$, $J_- = 0$, $J_z = 0$ and with a local maximum at the origin $(0, 0)$ and the continuum set of minima at the unit circle $x^2 + y^2 = 1$. For another choice of parameters, $J_+ = -1.5$, $J_- = -1.5$ and $J_z = 1.5$, in figure 3(b) this surface has a local minimum at the origin $(0, 0)$ and two local maxima at $(\pm 1, 0)$.

For the state $|G_-\rangle$ the energy is a constant which is independent of ψ:

$$\langle G_-|H|G_-\rangle = -\left(\frac{J_z}{2} + J_+\right). \tag{118}$$

6.2. Three-qubit energy for the XYZ model

Our set of two-qubit coherent states can be generalized to the multiple qubit case. Here we consider the three-qubit coherent state

$$|PG_+\rangle = \frac{1}{\sqrt{2}}(|\psi\rangle|\psi\rangle|\psi\rangle + |-\psi^*\rangle|-\psi^*\rangle|-\psi^*\rangle). \tag{119}$$

This state can be obtained from the maximally entangled GHZ state

$$|\mathrm{GHZ}\rangle = \frac{1}{\sqrt{2}}(|000\rangle + |111\rangle) \tag{120}$$

by unitary transformation $U_{123} = U \otimes U \otimes U$. This state is also maximally entangled (it can be seen by calculating the concurrence hyper-determinant) and in special cases $\psi \to 0$ and $\psi^* \to \infty$ reduces to the GHZ state.

The average energy of the XYZ model in this state is

$$\langle PG_+|H|PG_+\rangle = \frac{4J_+|\psi|^2(1+|\psi|^2) + 2J_-(1+|\psi|^2)(\psi^2+\bar{\psi}^2) + J_z(1-|\psi|^2-|\psi|^4+|\psi|^6)}{(1+|\psi|^2)^3}. \tag{121}$$

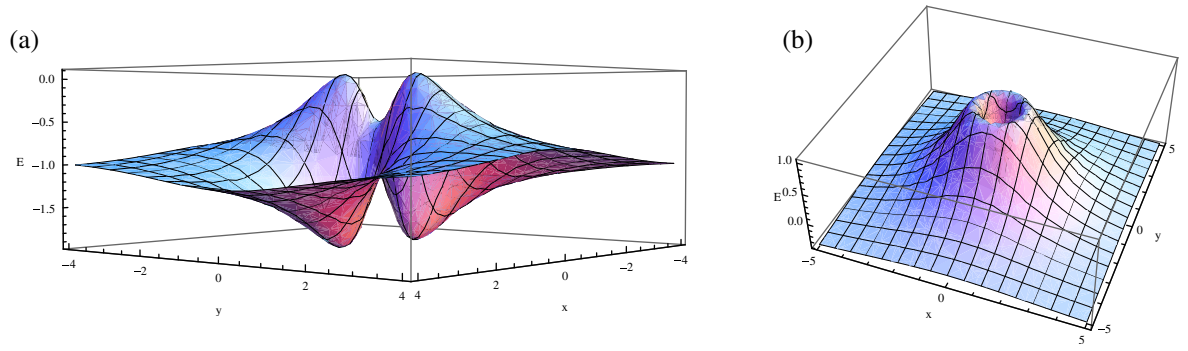

Figure 4. The average energy of the XYZ model in the maximally entangled three-qubit state $|PG_+\rangle$: (a) for $J_+ = -1$, $J_- = -1$ and $J_z = -1$; (b) for $J_+ = 1$, $J_- = 0$ and $J_z = -0.5$.

In figure 4(a), for $J_+ = -1$, $J_- = -1$ and $J_z = -1$, this energy surface has two local maxima at $(\mp 1, 0)$ and two local minima at $(0, \pm 1)$. For $J_+ = 1$, $J_- = 0$ and $J_z = -0.5$ in the same state, see figure 4(b), we plot the energy with local minimum at the origin $(0, 0)$ and with a continuous set of maxima at the unit circle $x^2 + y^2 = 1$.

Another three-qubit coherent state

$$|PG_-\rangle = \frac{1}{\sqrt{3}}\left(|\psi\rangle|\psi\rangle|-\psi^*\rangle + |\psi\rangle|-\psi^*\rangle|\psi\rangle + |-\psi^*\rangle|\psi\rangle|\psi\rangle\right) \tag{122}$$

is related to the maximally entangled $|W\rangle$ state

$$|W\rangle = \frac{1}{\sqrt{3}}\left(|0\rangle|0\rangle|1\rangle + |0\rangle|1\rangle|0\rangle + |1\rangle|0\rangle|0\rangle\right). \tag{123}$$

For the average energy in this state, we have

$$\langle PG_-|H|PG_-\rangle = \frac{4J_+(1+|\psi|^6) - 6J_-(1+|\psi|^2)(\psi^2+\bar{\psi}^2) - J_z(1-9|\psi|^2-9|\psi|^4+|\psi|^6)}{3(1+|\psi|^2)^3}. \tag{124}$$

The 3D plot of this energy in figure 5 shows two local maxima at $(\pm 1, 0)$ and a local minimum at the origin $(0, 0)$.

In all the above-considered examples, the average energy of the XYZ model is a function of two variables which determine the energy surface in two- or three-qubit phase space. At every point of this space, characterized by the complex number ψ, the quantum state is maximally entangled. And depending on the parameters of the system as exchange integrals J_x, J_y, J_z, it shows a specific shape with local maxima and minima at particular states. The dependence of these maxima and minima on external parameters such as magnetic field, or on the anisotropic exchange DM interaction, as well as on the number of qubits is worth studying.

7. Entanglement and fidelity of coherent state evolution

Some recent studies of the stability of quantum information processing focused on the fidelity and entanglement of the quantum evolution under the influence of impurities and the environment, as an indicator of the quality of the computation. These types of calculations

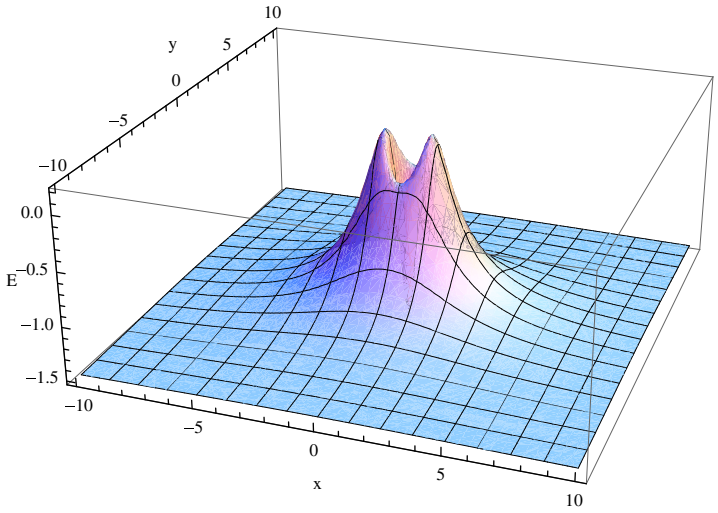

Figure 5. The average energy of the XYZ model in the $|PG_-\rangle$ state for $J_+ = -1$, $J_- = -0.2$ and $J_z = 0.5$.

were performed for different physical systems and for different initial states. Here, as a simple application of our two-qubit coherent states, we calculate the exact evolution in time of the entanglement and fidelity and their dependence on the initial coherent state parameters. By the evolution operator $U(t) = \exp[-\frac{\mathrm{i}}{\hbar}Ht]$ we first study the entanglement evolution for an initially maximally entangled two-qubit coherent state $|P_+\rangle$, (84). For simplicity, we display here only the particular case of the XX model. The time evolution of this state is

$$\begin{aligned}|\psi(t)\rangle &= U|P_+\rangle \\ &= \frac{1}{\sqrt{2}(1+|\psi|^2)}[(1+\bar{\psi}^2)|00\rangle + \mathrm{e}^{\frac{-\mathrm{i}Jt}{\hbar}}(\psi-\bar{\psi})|01\rangle \\ &\quad + \mathrm{e}^{\frac{-\mathrm{i}Jt}{\hbar}}(\psi-\bar{\psi})|10\rangle + (1+\psi^2)|11\rangle]. \end{aligned} \tag{125}$$

By the determinant formula (100) for concurrence we have the time dependence

$$\begin{aligned}C(t) &= 2|t_{00}t_{11} - t_{01}t_{10}| \\ &= \left|\frac{(1+\bar{\psi}^2)(1+\psi^2) - \mathrm{e}^{-\frac{2\mathrm{i}Jt}{\hbar}}(\psi-\bar{\psi})^2}{(1+|\psi|^2)^2}\right|. \end{aligned} \tag{126}$$

In polar coordinates for $\psi = r\mathrm{e}^{\mathrm{i}\theta}$ it gives

$$C(t) = \sqrt{1 - \frac{16r^2\sin^2\theta}{(1+r^2)^2}\left(1 - \frac{4r^2\sin^2\theta}{(1+r^2)^2}\right)\sin^2\frac{Jt}{\hbar}}. \tag{127}$$

This concurrence is a periodic function in t with revival times at $t = \frac{n\pi\hbar}{J}$, $n = 1, 2, \ldots$, when the concurrence returns to the maximal value $C = 1$. It is also the periodic function of θ shown in figures 6 and 7. The contour plot of the concurrence for different amplitudes $r = 0.4$, $r = 0.6$ and $r = 1$ undergoes dimerization of the periodic pattern in angle θ, from four columns at $r = 1$ to two columns for $r = 0.4$.

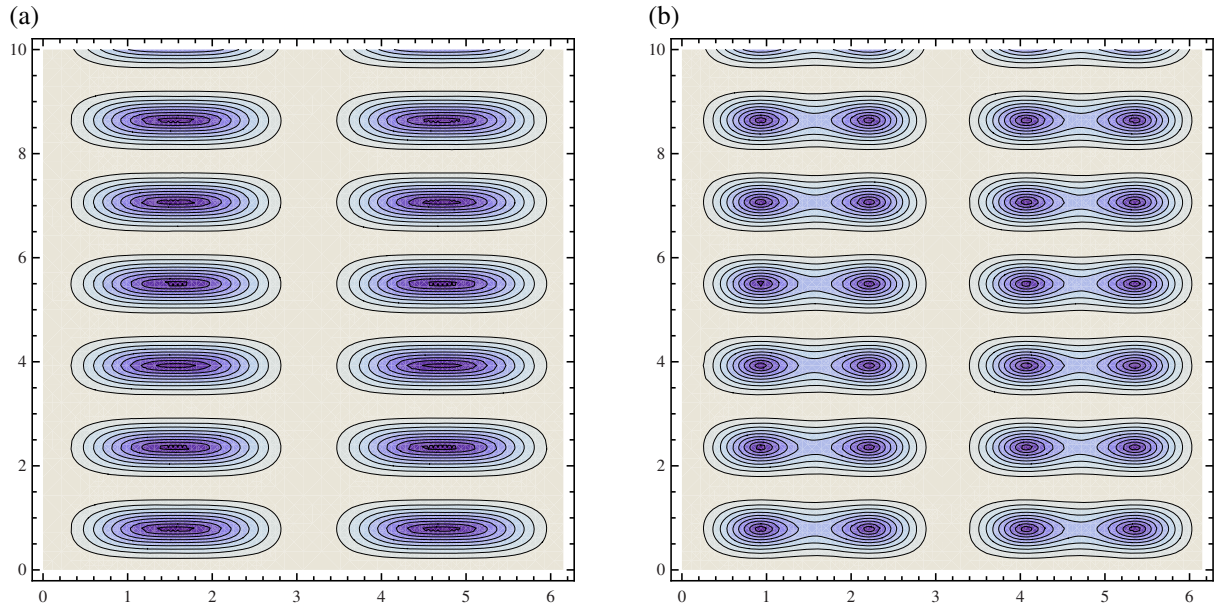

Figure 6. Contour plots of the concurrence versus θ (the horizontal axis) and t (the vertical axis): (a) for amplitude $r = 0.4$ and (b) for amplitude $r = 0.6$.

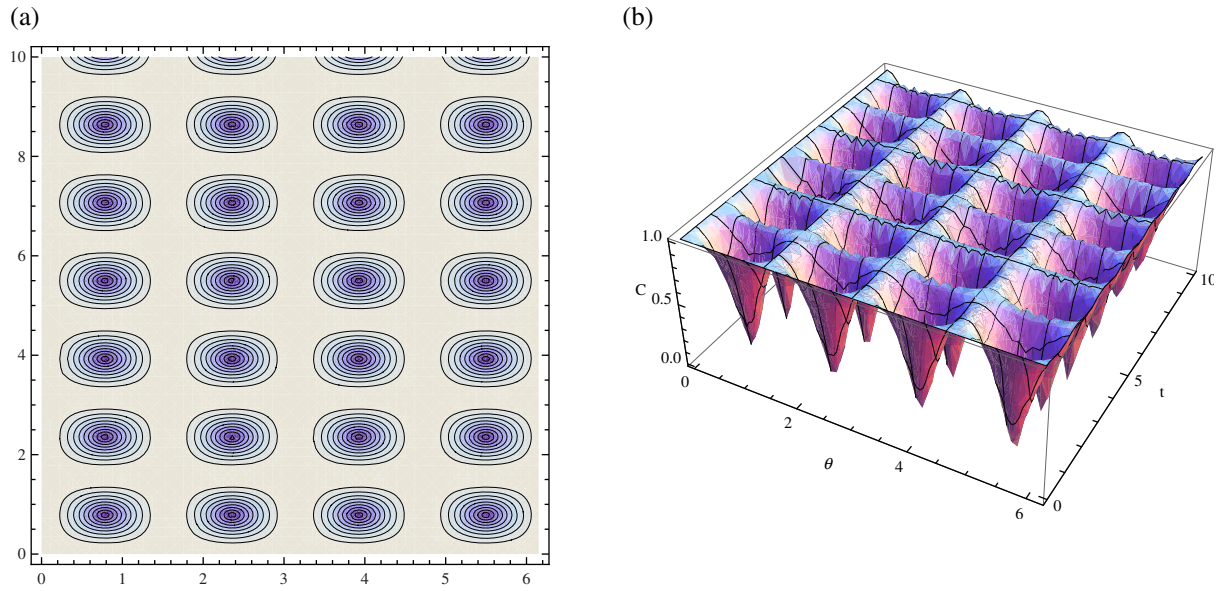

Figure 7. The concurrence versus θ (horizontal axis) and t (vertical axis) for amplitude $r = 1$: (a) the contour plot, (b) the 3D plot.

For the fidelity

$$F(t) = |\langle\psi(t)|P_+\rangle|^2 = \left|\frac{|(1+\bar{\psi}^2|^2 + e^{\frac{iJt}{\hbar}}|\psi - \bar{\psi}|^2}{(1+|\psi|^2)^2}\right|^2, \tag{128}$$

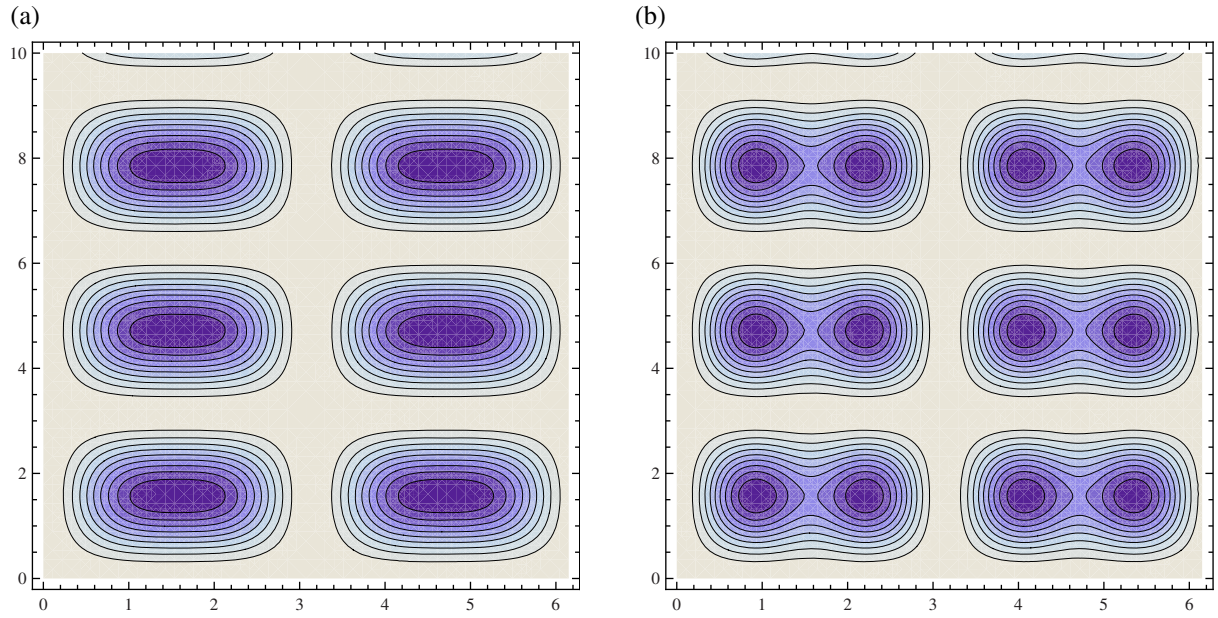

Figure 8. The contour plots of fidelity versus θ (horizontal axis) and t (vertical axis): (a) for amplitude $r = 0.4$, (b) for amplitude $r = 0.6$.

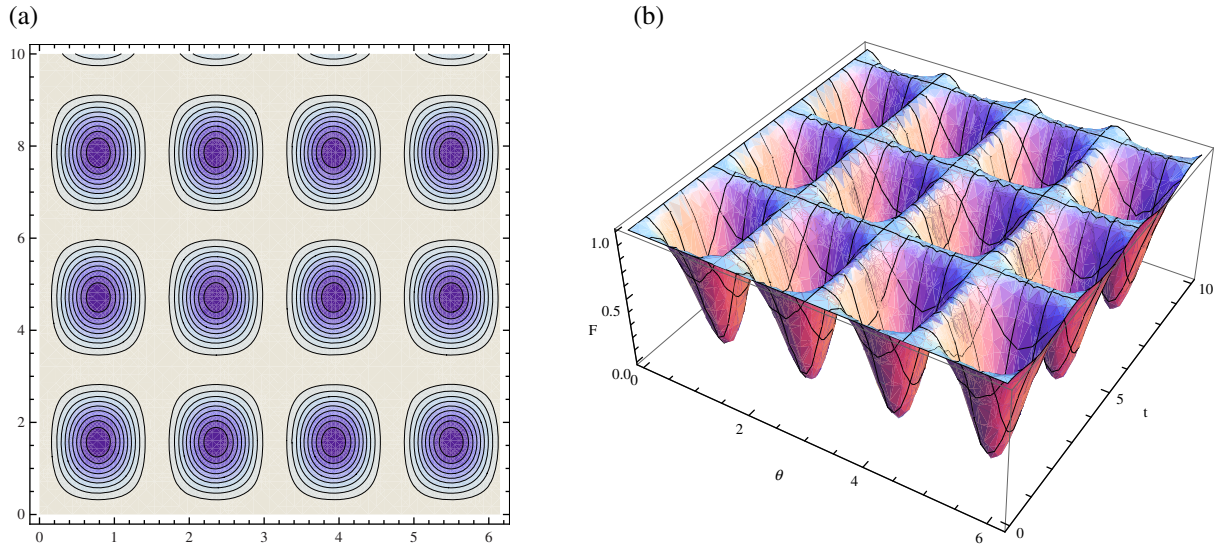

Figure 9. The fidelity versus θ (horizontal axis) and t (vertical axis) for amplitude $r = 1$: (a) the contour plot and (b) the 3D plot.

by parametrization $\psi = re^{i\theta}$ we have

$$F(t) = 1 - \frac{16r^2 \sin^2\theta}{(1+r^2)^2}\left(1 - \frac{4r^2\sin^2\theta}{(1+r^2)^2}\right)\sin^2\frac{Jt}{2\hbar}, \tag{129}$$

This also shows revival but at times $t = \frac{2n\pi\hbar}{J}$, $n = 1, 2, \ldots$, when the evolved state returns to the maximally entangled coherent state $|P_+\rangle$. We display this evolution in figures 8 and 9. Similarly to the concurrence case, we have the peridoic pattern in θ, so that at $r = 1$ we have

four columns merging with two columns at $r = 0.4$. But compared with concurrence, the fidelity revival time is twice as long.

The time evolution of concurrence and fidelity has been computed before for a spin model with different initial states [23], and it is not a new idea; here we did similar calculations for our two-qubit spin coherent states and found dimerization of the double periodic patterns versus r and θ in the complex plane ψ.

8. Conclusions

In this paper we introduced the set of maximally entangled two- and three-qubit coherent states, determined by antipodal points on the Bloch sphere. In the complex plane, these states are related to negative-symmetrical points with respect to the unit circle and can be interpreted as some type of source and its image states, similar to the hydrodynamic vortex case [20]. Then we can interpret these quantum states as a qubit and its image qubit, realizing some kind of method of images in the quantum theory.

The procedure described here can be extended also to construct multi-qubit coherent states. In this case, the states are characterized by complex Fibonacci and Lucas polynomials [24]. Entanglement properties of these states are under investigation. An interesting question here is to construct the average energy as a function of phase space variables. We expect that the energy surface in the multi-qubit case will show a specific localized structure with a number of local maxima and minima connected to the number of qubits. One interesting question is related to the characterization of entanglement for the continuous-variable case, which attracted attention recently in the teleportation of coherent states. Quantification of entanglement for these Gaussian states was completely characterized. In contrast to the Glauber bosonic coherent states, the spin coherent states considered in this paper are non-Gaussian states. For these states entanglement properties are fully characterized by the Schmidt coefficients of these states. It is well known that by the Holstein–Primakoff representation, as a basic tool to study magnons, the spin operators can be mapped to bosonic creation and annihilation operators. Then for a large spin j one can map our coherent states to the full Fock space by identifying $|j, m-j\rangle$ with the Fock state $|m\rangle$, for $m = 0, 1, \ldots, 2j$. Then by introducing $a = \sum_n \sqrt{n}|n-1\rangle\langle n|$ and continuous variables as coordinate and momentum $X = (a + a^+)/\sqrt{2}$, $P = (a - a^+)/\mathrm{i}\sqrt{2}$, one can compute the covariances and check the separability criteria of [11, 12]. Although this seems to be a cumbersome procedure it could shed some light on entanglement quantification for non-Gaussian continuous-variable states.

Acknowledgments

This work was supported by the National Research Foundation, the Ministry of Education, Singapore and the Izmir Institute of Technology, Turkey. The authors thank G Giedke for helpful comments and the referees for constructive remarks.

References

[1] Schrödinger E 1926 *Naturwissenschaften* **14** 664
[2] Glauber R J 1963 *Phys. Rev.* **131** 2766

[3] Perelomov A M 1972 Coherent states for arbitrary Lie groups *Commun. Math. Phys.* **26** 222–36
[4] Pashaev O K, Makhankov V G and Sergeenkov S A 1985 *Dynamical Symmetry and Spin Waves of Isotropic Antiferromagnet* (*JINR Rapid Communications* No. 10–85) (Dubna, Moscow) p 45
[5] Makhanov V and Pashaev O K 1992 Integrable pseudospin models in condensed matter *Soviet Scientific Reviews—Section C, Mathematical Physics Reviews* vol 9, part 3 ed S P Novikov (Chur: Harwood Academic) pp 1–152
[6] Makhankov V and Pashaev O K 1988 Noncompact magnets and the Bogolyubov condensate *Acad. Sci. USSR Dokl.* **301** 1356–61
Makhankov V and Pashaev O K 1988 Noncompact magnets and the Bogolyubov condensate *Sov. Phys.—Dokl.* **33** 585–7 (Engl. transl.)
[7] Solomon A I 1971 *J. Math. Phys.* **12** 390
[8] Gochev I G 1984 *Phys. Lett.* A **104** 36
[9] Sanders B C 1992 *Phys. Rev.* A **45** 6811–5
[10] Furusawa A *et al* 1998 *Science* **282** 706
[11] Duan L M, Giedke G, Cirac J I and Zoller P 2000 *Phys. Rev. Lett.* **84** 4002
[12] Simon R 2000 *Phys. Rev. Lett.* **84** 2726
[13] Bhatt J R, Panigrahi P K and Vyas M 2008 *Phys. Rev.* A **78** 034101
[14] Fujii K 2002 arXiv:quant-ph/0112090
[15] Ahlfors L 1979 *Complex Analysis* 3rd edn (New York: McGraw-Hill)
[16] Dodonov V V, Man'ko V I and Nikonov D E 1995 *Phys. Rev.* A **51** 4 3328
[17] Perelomov A 1986 *Generalized Coherent States and their Applications* (New York: Springer)
[18] Milne-Thomson L M 1968 *Theoretical Hydrodynamics* (London: Macmillan)
[19] Poincare H 1893 *Theorie des Tourbillions* (Paris: Georges Carré)
[20] Pashaev O K and Yilmaz O 2008 *J. Phys. A: Math. Theor.* **41** 135207
[21] Klyachko A A and Shumovsky A S 2002 arXiv:quant-ph/0203099v1
[22] Lee J, Kim C H, Lee E K, Kim J and Lee S 2002 *Quantum Inf. Process.* **1** 129
[23] Shi Q Q *et al* 2007 arXiv:0706.2402v1
[24] Pashaev O K 2011 Vortex images, q-calculus and entangled coherent states *VIIth Int. Conf. on Quantum Theory and Symmetries (QTS7) (Prague, 7–13 August)*
Pashaev O K 2012 Vortex images, q-calculus and entangled coherent states *J. Phys.: Conf. Ser.* **343** 012093